Hindawi Publishing Corporation
International Journal of Antennas and Propagation
Volume 2014, Article ID 147341, 10 pages
http://dx.doi.org/10.1155/2014/147341

Research Article

Simulations and Measurements of Electric Fields Emitted from a LTE Base Station in an Urban Area

Hsing-Yi Chen and Tsung-Han Lin

Department of Communications Engineering, Yuan Ze University, 135 Yuan-Tung Road, Nei-Li, Chung-Li, Taoyuan Shian 320, Taiwan

Correspondence should be addressed to Hsing-Yi Chen; eehychen@saturn.yzu.edu.tw

Received 24 May 2014; Revised 28 July 2014; Accepted 26 August 2014; Published 13 October 2014

Academic Editor: Tamer S. Ibrahim

Radiation patterns emitted from a long-term evolution (LTE) base station antenna were first simulated by the finite-difference time domain (FDTD) method. The validity of simulation results of radiation patterns was further checked by measurement data. After validating the accuracy of the FDTD method, electric fields at 123 test sites around a LTE base station in an urban area of Taipei City were simulated. Simulated electric fields were also validated by comparison with measured data obtained by a high frequency selective radiation meter with an isotropic E-field probe. Simulated and measured electric fields are in the range of 0.104–1.182 and 0.098–1.179 V/m at 1795 MHz, respectively. From obtained electric field strengths, it is ensured that the urban area is a good signal environment. The maximum power density emitted from the LTE base station is about 1.853×10^{-4} mW/cm^2 and is thus far below the safety standard value of 1.197 mW/cm^2 for human exposure to RF radiation at 1795 MHz.

1. Introduction

Mobile broadband networks are becoming insufficient as operators offer widespread broadband multimedia access to meet the increased demand. Fortunately, the long-term evolution (LTE), known as the fourth generation wireless communication system, promises to meet the requirements of real time applications, advanced games and video downloading, and other ultrafast broadband services for mobile phones and data terminals. LTE is a technical specification used to enhance and to optimize the third Generation Partnership Project radio access architecture [1]. It is based on the global system for mobile communications (GSM) and the universal mobile telecommunications system (UMTS) network technologies to increase capacity and speed using a different radio interface together with core network improvements [2, 3]. Its spectrum includes LTE 700, GSM 850, GSM 900, DCS 1800, PCS 1900, WCDMA 2100, LTE B7 (2.5–2.69 GHz), LTE B38 (2.57–2.62 GHz), and LTE B40 (2.3-2.4 GHz). Taiwan's National Communications Commission (NCC) decided to issue 6 LTE licenses on October 31st, 2013. The spectrum offered by the NCC was in the 700, 900, and 1800 MHz frequency bands.

To meet the demand for LTE communication with extended coverage, high cell capacity, and high data rates, the number of LTE base stations will also increase sharply. With the increased number of LTE base stations, the possible health hazards are a matter of concern for people in Taiwan due to exposure to electromagnetic (EM) radiation from LTE base stations. In recent years, some residents near cellular phone base stations have reported feeling several unspecific symptoms including fatigue, sleep disturbance, dizziness, loss of mental attention, and headaches. However, there is no convincing scientific evidence that the EM fields emitted from cellular phone base stations cause adverse health effects.

On the other hand, EM field intensities at users' locations should be guaranteed above a threshold level in order to meet the best RF (radio frequency) condition where it is free from interference. However, EM field intensities drop rapidly as the distance increases from a LTE base station because of the attenuation of power with the square of distance. Consequently, it is an important trade-off issue for RF engineers to determine the safety distance for EM radiation from a LTE base station and also to keep EM field intensity above a threshold level. Some advisory authorities have recommended safety guidelines for human exposure

to EM energy. These authorities include the Institute of Electrical and Electronics Engineers and American National Standards Institute (IEEE/ANSI) [4], the International Commissions on Non-Ionizing Radiation Protection (ICNIRP) [5], and the National Council on Radiation Protection and Measurements (NCRP) [6]. For example, for human exposure in uncontrolled environments to EM energy at radio frequencies from 300 MHz to 15 GHz, the ANSI/IEEE safety standard is expressed by $f/1500\,\mathrm{mW/cm^2}$, where frequency f is in MHz. Measurements of RF electric and magnetic fields around cellular phone base stations may be available in the literature [7–9]. There are only a few reports regarding theoretical studies on electric field strengths near cellular phone base stations [10]. In this paper, the finite-difference time-domain (FDTD) method [11] and the near zone to far zone transformation technique [12] were used to calculate electric fields emitted from a LTE base station constructed on the roof-floor of a building with a height of 29 meters in an urban area of Taipei City. The validity of the FDTD method and the near zone to far zone transformation technique was checked by comparing numerical results of radiation patterns of a LTE base station antenna with those obtained by the measuring method in Yuan Ze anechoic chamber. Simulated electric fields at 123 test sites around the LTE base station in the urban area were also compared with measurement data and safety standard levels recommended by the IEEE/ANSI.

2. Brief Description of FDTD

The FDTD method was first presented by Yee [11] for solving Maxwell's curl equations directly in the time domain on a spatial grid in 1966 and later developed by many researchers for antenna analysis, electromagnetic interference (EMI), EM wave propagation and scattering problems, design of microwave and optical circuits, EM biological effects, defense applications, and many electromagnetic problems. In the FDTD solution procedure, six components of EM fields E and H are each positioned in discrete half spatial step intervals around a unit cell and the coupled Maxwell equations in differential form are solved for various points of the target as well as the surrounding in a time-stepping manner until converged solutions are obtained. Following Yee's notation and using centered difference approximation on both of the time and space first-order partial differentiations, six coupled scalar finite-difference equations for six unique field components within a unit cell are obtained. In these six coupled scalar finite-difference equations, electric fields are assigned to half-integer $(n + (1/2))$ time steps and magnetic fields are assigned to integer (n) time steps for the temporal discretization of fields. Two of the six coupled scalar finite-difference equations are shown in

$$\begin{aligned}
&\widetilde{E}_x^{n+1}\left(i+\frac{1}{2},j,k\right)\\
&\quad=\mathrm{CA}_x\left(i+\frac{1}{2},j,k\right)\widetilde{E}_x^{n}\left(i+\frac{1}{2},j,k\right)+\mathrm{CB}_x\left(i+\frac{1}{2},j,k\right)\\
&\qquad\times\left[H_z^{n+(1/2)}\left(i+\frac{1}{2},j+\frac{1}{2},k\right)\right.\\
&\qquad\quad-H_z^{n+(1/2)}\left(i+\frac{1}{2},j-\frac{1}{2},k\right)\\
&\qquad\quad+H_y^{n+(1/2)}\left(i+\frac{1}{2},j,k-\frac{1}{2}\right)\\
&\qquad\quad\left.-H_y^{n+(1/2)}\left(i+\frac{1}{2},j,k+\frac{1}{2}\right)\right],\\
&H_x^{n+(1/2)}\left(i,j+\frac{1}{2},k+\frac{1}{2}\right)\\
&\quad=H_x^{n-(1/2)}\left(i,j+\frac{1}{2},k+\frac{1}{2}\right)\\
&\qquad+\left(\frac{\mathrm{RC}}{\mu_{rx}\left(i,j+(1/2),k+(1/2)\right)}\right)\\
&\qquad\times\left[\widetilde{E}_y^{n}\left(i,j+\frac{1}{2},k+1\right)-\widetilde{E}_y^{n}\left(i,j+\frac{1}{2},k\right)\right.\\
&\qquad\quad\left.+\widetilde{E}_z^{n}\left(i,j,k+\frac{1}{2}\right)-\widetilde{E}_z^{n}\left(i,j+1,k+\frac{1}{2}\right)\right],
\end{aligned}\tag{1}$$

where

$$\begin{aligned}
&\mathrm{CA}_x\left(i+\frac{1}{2},j,k\right)\\
&\quad=\frac{2\varepsilon_x\left(i+(1/2),j,k\right)-\sigma_x\left(i+(1/2),j,k\right)\delta_t}{2\varepsilon_x\left(i+(1/2),j,k\right)+\sigma_x\left(i+(1/2),j,k\right)\delta_t},\\
&\mathrm{CB}_x\left(i+\frac{1}{2},j,k\right)\\
&\quad=\frac{2\varepsilon_0\mathrm{RC}}{2\varepsilon_x\left(i+(1/2),j,k\right)+\sigma_x\left(i+(1/2),j,k\right)\delta_t},\\
&\mathrm{RC}=\frac{\delta_t}{\delta\left(\mu_0\varepsilon_0\right)^{1/2}}=0.5,
\end{aligned}\tag{2}$$

where ε_0 is the permittivity of free space, μ_0 is the permeability of free-space, μ_{rx} is the relative permeability, ε_x is the permittivity, and σ_x is the conductivity of the media at respective locations. The normalized electric field in (1) is defined by $\widetilde{E}=(\varepsilon_0/\mu_0)^{1/2}E$. The time step δ_t is set to $\delta/(2C_o)$ [13], where δ and C_o are the cell size and the speed of light, respectively, to ensure numerical stability.

An important issue encountered in the FDTD method is the absorbing boundary conditions (ABC). They are applied to truncate the computational domain when modeling an open region problem. Several ABC techniques have been proposed in the FDTD method such as second-order Mur [14], and Liao [15] and perfectly matched layer (PML) [16]. Liao ABC and PML require a lot of memory. Second-order Mur absorbing boundary conditions are the most commonly used grid truncation techniques. In our formulation, the second-order Mur absorbing boundary conditions are used for the near-field emission problems. The second-order Mur absorbing boundaries are employed because they do not require much memory and have a reasonable accuracy. For near-field applications, the FDTD computation space has

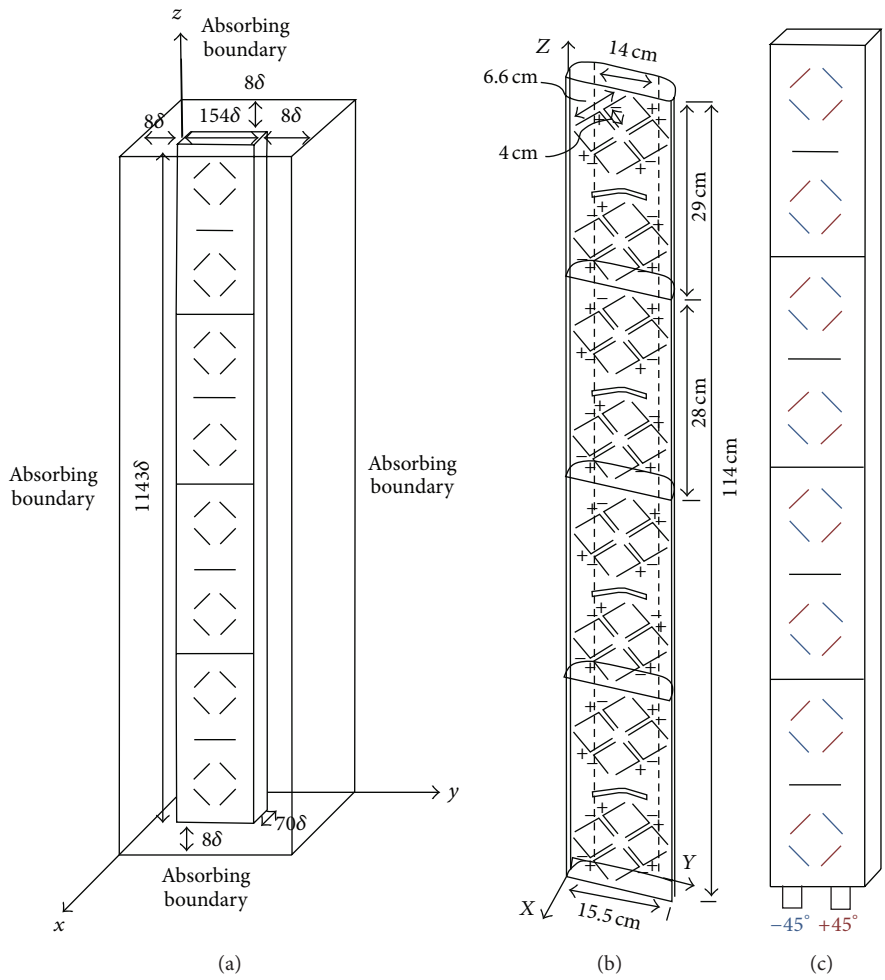

Figure 1: (a) FDTD model with $86 \times 170 \times 1159 = 16,944,580$ cubic cells. The cell size is 1 mm. (b) Relative locations of 32 radiators. (c) Illustration of two identical feeding lines excited by different phases of +45° (red line) and −45° (blue line).

only one region; that is, there is no scattering region, as shown in Figure 1(a). In order to reduce the FDTD model space, it is desirable to bring the absorbing boundaries as close to the region of interest as possible. In general, the external absorbing boundaries are placed at a distances of 5–8δ on all sides of the scattering object. In this study, the external absorbing boundaries are placed at a distance of 8δ on all sides of the scattering target as shown in Figure 1, where δ is the cell size.

3. EM Fields Emitted from Antenna Radome

Applying the field equivalence principle [17–20], electromagnetic fields in space due to equivalent sources at the emitting surface S can be obtained from electric and magnetic surface currents flowing on S, where electric and magnetic surface currents are equivalent to tangential magnetic and electric fields at the emitting surface S, respectively. Based on the equivalence principle, if the tangential electric and magnetic fields are completely known over the LTE antenna radome surface, the electric and magnetic fields in the source-free region can be determined.

As the electric and magnetic fields in the radome are determined by the FDTD method, the electric and magnetic current densities on the surface of the radome can be obtained from boundary conditions expressed by

$$\begin{aligned} \overrightarrow{J}_{\text{es}} &= \vec{n} \times \left(\overrightarrow{H}_{\text{air}} - \overrightarrow{H}_{\text{radome}}\right)\Big|_{\overrightarrow{H}_{\text{air}}=0} = -\overrightarrow{n} \times \overrightarrow{H}_{\text{radome}}, \\ \overrightarrow{J}_{\text{ms}} &= -\vec{n} \times \left(\overrightarrow{E}_{\text{air}} - \overrightarrow{E}_{\text{radome}}\right)\Big|_{\overrightarrow{E}_{\text{air}}=0} = \overrightarrow{n} \times \overrightarrow{E}_{\text{radome}}, \end{aligned} \tag{3}$$

where $\overrightarrow{J}_{\text{es}}$ and $\overrightarrow{J}_{\text{ms}}$ are the electric and magnetic current densities on the surface of the radome, $\overrightarrow{E}_{\text{air}}$ and $\overrightarrow{H}_{\text{air}}$ are the electric and magnetic fields in air, $\overrightarrow{E}_{\text{radome}}$ and $\overrightarrow{H}_{\text{radome}}$ are the electric and magnetic fields in the radome, and $\overrightarrow{n}$ is a unit vector outward from the radome to the air. We can find the electric and magnetic fields in air generated by the electric

and magnetic current densities $\overrightarrow{J}_{\text{es}}$ and $\overrightarrow{J}_{\text{ms}}$. Using far-field conditions, the $\overrightarrow{E}$- and $\overrightarrow{H}$-fields can be written as [18, 20]

$$\begin{aligned} E_r &= 0, \\ E_\theta &= -\frac{jk_0 e^{-jk_0 r}}{4\pi r}\left(L_\phi + \eta_0 N_\theta\right), \\ E_\phi &= \frac{jk_0 e^{-jk_0 r}}{4\pi r}\left(L_\theta - \eta_0 N_\phi\right), \\ H_r &= 0, \\ H_\theta &= \frac{jk_0 e^{-jk_0 r}}{4\pi r}\left(N_\phi - \frac{L_\theta}{\eta_0}\right), \\ H_\phi &= -\frac{jk_0 e^{-jk_0 r}}{4\pi r}\left(N_\theta + \frac{L_\phi}{\eta_0}\right), \end{aligned} \tag{4}$$

where

$$\eta_0 = \sqrt{\frac{\mu_0}{\varepsilon_0}}. \tag{5}$$

The N_θ, N_ϕ, L_θ, and L_ϕ can be obtained by

$$\begin{aligned} N_\theta &= \iint_s \left[J_{esx}\cos\theta\cos\phi + J_{esy}\cos\theta\sin\phi - J_{esz}\sin\theta\right] \\ &\quad \times e^{jk_0 r'\cos\varphi}\, ds', \\ N_\phi &= \iint_s \left[-J_{esx}\sin\phi + J_{esy}\cos\phi\right] e^{jk_0 r'\cos\varphi}\, ds', \\ L_\theta &= \iint_s \left[J_{msx}\cos\theta\cos\phi + J_{msy}\cos\theta\sin\varphi - J_{msz}\sin\theta\right] \\ &\quad \times e^{jk_0 r'\cos\varphi}\, ds', \\ L_\phi &= \iint_s \left[-J_{msx}\sin\phi + J_{msy}\cos\phi\right] e^{jk_0 r'\cos\varphi}\, ds', \end{aligned} \tag{6}$$

where θ and ϕ are the polar and azimuthal angles defined in a spherical coordinate system. Consider

$$\begin{aligned} \overrightarrow{J}_{\text{es}} &= J_{esx}\hat{a}_x + J_{esy}\hat{a}_y + J_{esz}\hat{a}_z, \\ \overrightarrow{J}_{\text{ms}} &= J_{msx}\hat{a}_x + J_{msy}\hat{a}_y + J_{msz}\hat{a}_z. \end{aligned} \tag{7}$$

4. Scattered Fields of the Ground and Building

The induced electric fields in the ground and buildings can be obtained by using the computation procedure described in Section 3 and boundary conditions. From boundary conditions, the tangential component of an electric field is continuous and the normal component of an electric flux is discontinuous across an interface. However, the normal component of an electric flux is enforced tobe continuous since the surface charge density on the ground and buildings is negligible. As the induced electric fields in the ground and buildings are obtained, the equivalent current density $\vec{J}_{\text{eq}}$ [21] in the ground and buildings can be computed by

$$\overrightarrow{J}_{\text{eq}} = \left[\sigma + j\omega\varepsilon_0\left(\varepsilon_r - 1\right)\right]\overrightarrow{E}\left(r'\right), \tag{8}$$

where $\overrightarrow{E}(r')$ is the electric field in the ground and buildings, ω is the angular frequency, ε_r and σ denote the relative dielectric constants and conductivities of the ground and buildings, respectively. The first term of (8) is the conduction current and the second term represents the polarization current. Therefore, the electric field $\overrightarrow{E}^s$ scattered from the ground or buildings can be obtained from the equivalent current density expressed as [22]

$$\overrightarrow{E}^s\left(\overrightarrow{r}\right) = -j\eta_0 k_0 \int_v \overrightarrow{J}_{\text{eq}}\left(r'\right)\cdot\left[\overleftrightarrow{I} + \frac{\nabla\nabla}{k_0^2}\right] G_0\left(\overrightarrow{r}, \overrightarrow{r}'\right) dv', \tag{9}$$

where

$$\begin{aligned} G_0\left(\overrightarrow{r}, \overrightarrow{r}'\right) &= \frac{\exp\left(-jk_0 R\right)}{4\pi R}, \\ R &= \left|\overrightarrow{r} - \overrightarrow{r}'\right| = \sqrt{(x-x')^2 + (y-y')^2 + (z-z')^2}, \\ \eta_0 &= \sqrt{\frac{\mu_0}{\varepsilon_0}}, \\ k_0 &= \omega\sqrt{\mu_0\varepsilon_0}. \end{aligned} \tag{10}$$

In the above equations, $\overleftrightarrow{I}$ is the identity tensor, $\varepsilon_0 = 8.854 \times 10^{-12}$ F/m is the permittivity of free space, $\mu_0 = 4\pi\times10^{-7}$ H/m is the permeability of free space, k_0 is the wave propagation constant of free space, and $\overrightarrow{r}(x, y, z)$ and $\overrightarrow{r}'(x', y', z')$ are field position vector and source position vector, respectively. For far-field approximation, $k_0 R \gg 1$, $\overrightarrow{r} \gg \overrightarrow{r}'$, and $\overrightarrow{r}//\overrightarrow{R}'$, a simpler formula for the integral equation (9) can be obtained by

$$\overrightarrow{E}^s\left(\overrightarrow{r}\right) = -j\eta_0 k_0 \int_v \left[J_\theta\left(\overrightarrow{r}'\right)\overrightarrow{a}_\theta + J_\phi\left(\overrightarrow{r}'\right)\overrightarrow{a}_\phi\right]\frac{e^{-jk_0 R}}{4\pi R}\, dv', \tag{11}$$

where θ and ϕ are the polar and azimuthal angles defined in a spherical coordinate system and $\overrightarrow{a}_\theta$ and $\overrightarrow{a}_\phi$ are unit vectors, respectively. The transformations between rectangular and spherical components for $\overrightarrow{a}_r$, $J_\theta(\overrightarrow{r}')$, and $J_\phi(\overrightarrow{r}')$ are given by

$$\begin{aligned} \overrightarrow{a}_r &= \sin\theta\cos\phi\overrightarrow{a}_x + \sin\theta\sin\phi\overrightarrow{a}_y + \cos\theta\overrightarrow{a}_z, \\ J_\theta\left(\overrightarrow{r}'\right) &= J_x\left(\overrightarrow{r}'\right)\cos\theta\cos\phi + J_y\left(\overrightarrow{r}'\right)\cos\theta\sin\phi \\ &\quad - J_z\left(\overrightarrow{r}'\right)\sin\theta, \\ J_\phi\left(\overrightarrow{r}'\right) &= -J_x\left(\overrightarrow{r}'\right)\sin\phi + J_y\left(\overrightarrow{r}'\right)\cos\phi. \end{aligned} \tag{12}$$

The scattered far-field components E_θ and E_ϕ can easily be found by calculating the far-field radiated from currents distributed in the ground and buildings as presented in [20]

$$\begin{aligned}\vec{E}^s(\theta,\phi) &= E_\theta \overrightarrow{a}_\theta + E_\phi \overrightarrow{a}_\phi \\ &= \frac{-j\eta_0 k_0}{4\pi r}\exp(-jk_0 r) \\ &\times \int_v \left\{\overrightarrow{a}_\theta \left[J_x(\vec{r}')\cos\theta\cos\phi \right.\right. \\ &\quad \left. + J_y(\vec{r}')\cos\theta\sin\phi - J_z(\vec{r}')\sin\theta\right] \\ &\quad \left. + \overrightarrow{a}_\phi \left[-J_x(\vec{r}')\sin\phi + J_y(\vec{r}')\cos\phi\right]\right\} \\ &\times \exp\left[jk_0\left(x'\sin\theta\cos\phi + y'\sin\theta\sin\phi \right.\right. \\ &\quad \left.\left. + z'\cos\theta\right)\right] dv',\end{aligned} \tag{13}$$

where η_0 is the wave impedance, k_0 is the wave propagation constant, $\vec{r}$ is the field position point, $\vec{r}'$ is the source position point, and $J_x(\vec{r}')$, $J_y(\vec{r}')$, and $J_z(\vec{r}')$ are the current densities flowing in the x-, y-, and z-axis inside the ground and buildings, respectively. Since EM waves can quickly decay in lossy materials, the integral equation (13) only takes into account a depth of 20 cm from the ground and the building surfaces as the volume space for calculations of scatter fields. In addition, only primary scattered fields from the ground and buildings are considered as contributing to the receiving fields at test sites.

5. The LTE Base Station Antenna

An overview of a LTE base station antenna is shown in Figure 2. The LTE base station antenna dimension is about 155 × 70 × 1143 mm^3 as shown in Figure 2(b). It is manufactured with an aluminum reflector screen and 32 tin-plated zinc radiators protected by a flat fiberglass radome as shown in Figure 1(b) [23]. The maximum radome depth is 70 mm. The 32 radiators are equally divided into two groups that are fed by two identical feeding lines with different excitation phases of +45° and −45° as shown in Figure 1(c). The LTE base station antenna has three frequency bands of 1710~1880, 1850~1990, and 1920~2170 MHz. Each feeding line has an impedance of 50 ohms operating at frequencies of 1710~2170 MHz. The LTE base station antenna is designed to have a radiation power of 1~300 watts. Due to the NCC regulation, a maximum radiation power of 20 watts is permissible for the LTE base station antenna to operate in urban areas. The metallic case of the LTE base station antenna and the mounting kit are DC grounded. Base station antennas with vertical down-tilting have some impact on the antenna performance such as gain, capacity, coverage, and interference [24–30]. In this study, the down-tilting angle of the LTE base station antenna is 8 degrees with respect to the vertical plane.

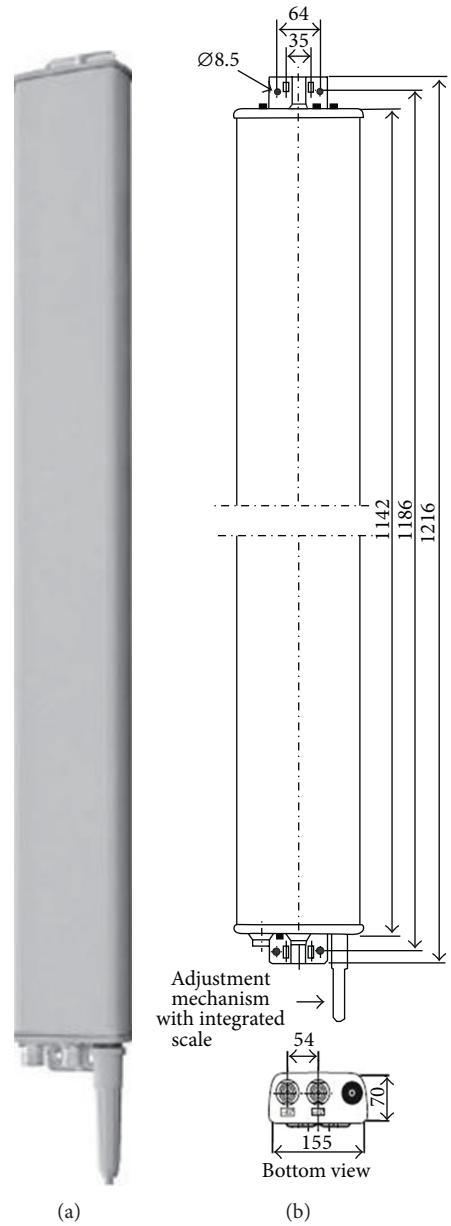

Figure 2: LTE base station antenna. (a) Antenna set. (b) Antenna dimensions (mm).

6. Simulation and Measurement

For FDTD simulations, the metallic material used for the LTE base station antenna is assumed to be nonmagnetic (μ_r = 1.0). The tangential components of electric and magnetic fields in the conducting case are enforced to zero. The LTE base station antenna is constructed with 16,944,580 cubic cells of 1.0 mm on each side. The maximum excitation source voltage V of 31.625 volts at the input port of each radiator emitting a power of 0.625 watts at frequencies of 1710~1880, 1850–1990, and 1920–2170 MHz is adopted for FDTD simulations. The excitation source voltage is then transferred into a sinusoidally modulated Gaussian pulse wave [31] over

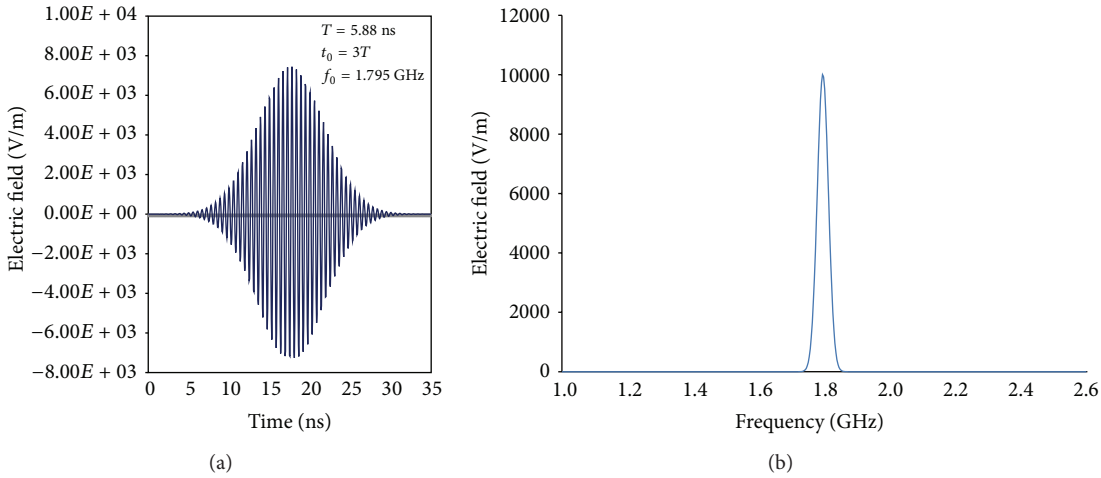

FIGURE 3: The sinusoidally modulated Gaussian pulse wave $E = E_0 \exp(-[(t - t_0)/T]^2) \sin 2\pi f_0(t - t_0)$, where $E_0 = 10,541$ V/m, $t_0 = 3T$, $T = 5.88 \times 10^{-9}$ s, and $f_0 = 1795$ MHz. (a) Time domain. (b) Frequency domain.

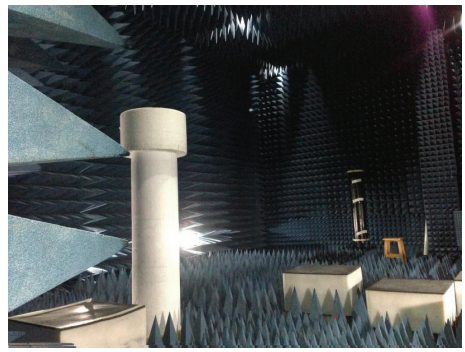

FIGURE 4: Measurements of radiation patterns in an anechoic chamber.

the gap between the two arms of each radiator by $E = E_0 \exp(-[(t - t_0)/T]^2) \sin 2\pi f_0(t - t_0)$, where $E_0 = (V/d)$ is the amplitude of the excited electric field, $t_0 = 3T$ is the center of the pulse, T denotes the pulse width at its $1/e$ characteristics decay point which is in terms of frequency bandwidth (BW) expressed by BW(GHz) $= 1000/T$(ps), f_0 is the center frequency (modulation frequency), $d = 3\delta$ is the distance of the gap between the two arms of each transmitter, and $\delta = 1$ mm is the cell size used in the FDTD. Figure 3 shows a sinusoidally modulated Gaussian pulse with pulse width $T = 5.88 \times 10^{-9}$ s and center frequency $f_0 = 1795$ MHz. The relative dielectric constants and electrical conductivities of conducting cases (iron), transmitters, and radome are adopted to be ($\varepsilon_r = 1.0$, $\sigma = 1.0 \times 10^7$ S/m), ($\varepsilon_r = 1.0$, $\sigma = 5.8 \times 10^7$ S/m), and ($\varepsilon_r = 2.5$, $\sigma = 7.01 \times 10^{-4}$ S/m) [32], respectively.

As the electric fields in the radome are calculated by the FDTD method, the scattered electric fields radiated from the ground and buildings can be obtained by using the computation procedures described in Sections 3 and 4. Finally, the electric fields at 123 test sites in an urban area of Taipei City can be obtained by adding the electric fields radiated directly from the LTE base station antenna and the scattered electric fields radiated from the ground and buildings.

The measurements of radiation patterns were performed in an anechoic chamber as shown in Figure 4 using an Anritsu 37369C Vector Network Analyzer and an Anritsu MS2687B spectrum analyzer. The distance between the LTE base station antenna and the receiving antenna was set at 6.5 meters for vertical and horizontal polarizations. Figures 5, 6, and 7 show measurement data and FDTD results of radiation patterns under the far-field condition for vertical and horizontal polarizations at frequencies of 1795, 1920, and 2060 MHz, respectively. From Figures 5–7, it is clear that the measurement data make a good agreement with simulation results. It is also found that the LTE base station antenna has an averaged beam width of about 120 degrees with −10 dB drop in the horizontal plane and about 7.5 degrees with −3 dB drop in the vertical plane for frequencies operating at 1795, 1920, and 2060 MHz, respectively. The LTE antenna has a narrow beam pattern in the vertical plane but quite wide beam pattern in the horizontal plane.

A model of an urban area of Taipei City having 123 test sites adopted for measuring electric fields emitted from a LTE base station is shown in Figure 8. The LTE base station antenna system employs a sector arrangement, with three sets of directional transmitting and receiving antennas oriented 120 degrees apart and aiming at the horizon. The

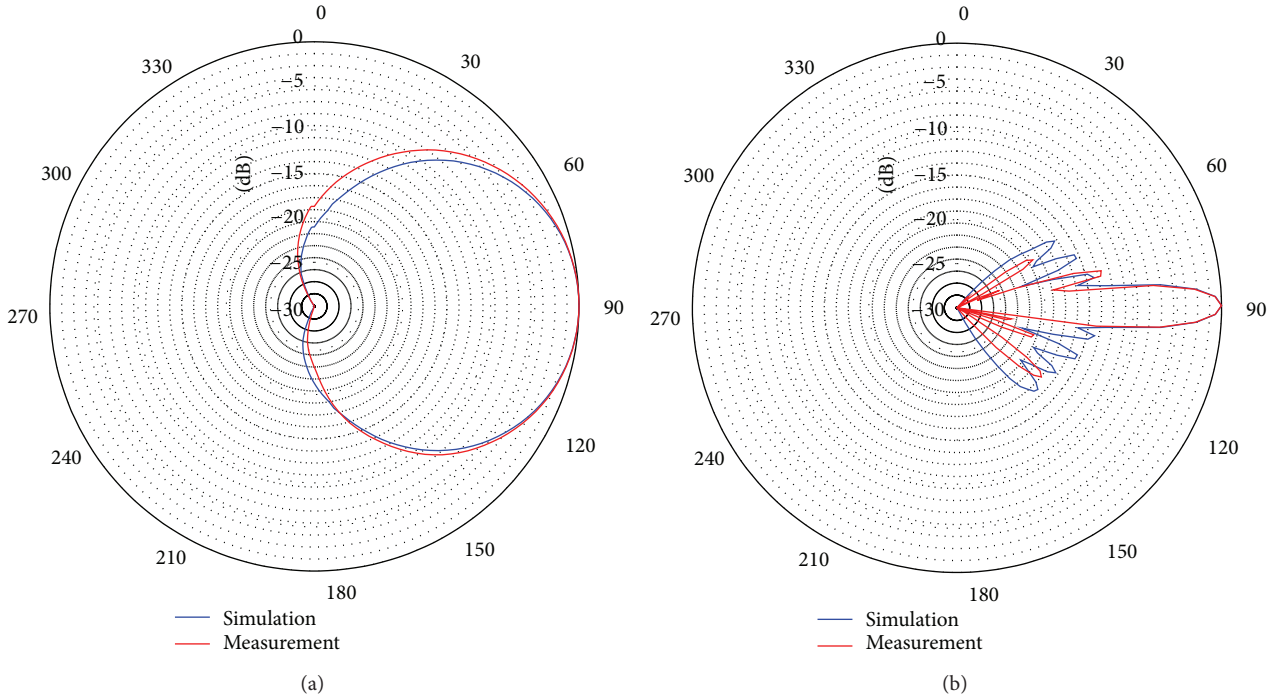

Figure 5: Comparison of radiation patterns at 1795 MHz on the horizontal and vertical planes obtained by FDTD method and measurement. (a) Horizontal plane (ϕ). (b) Vertical plane (θ).

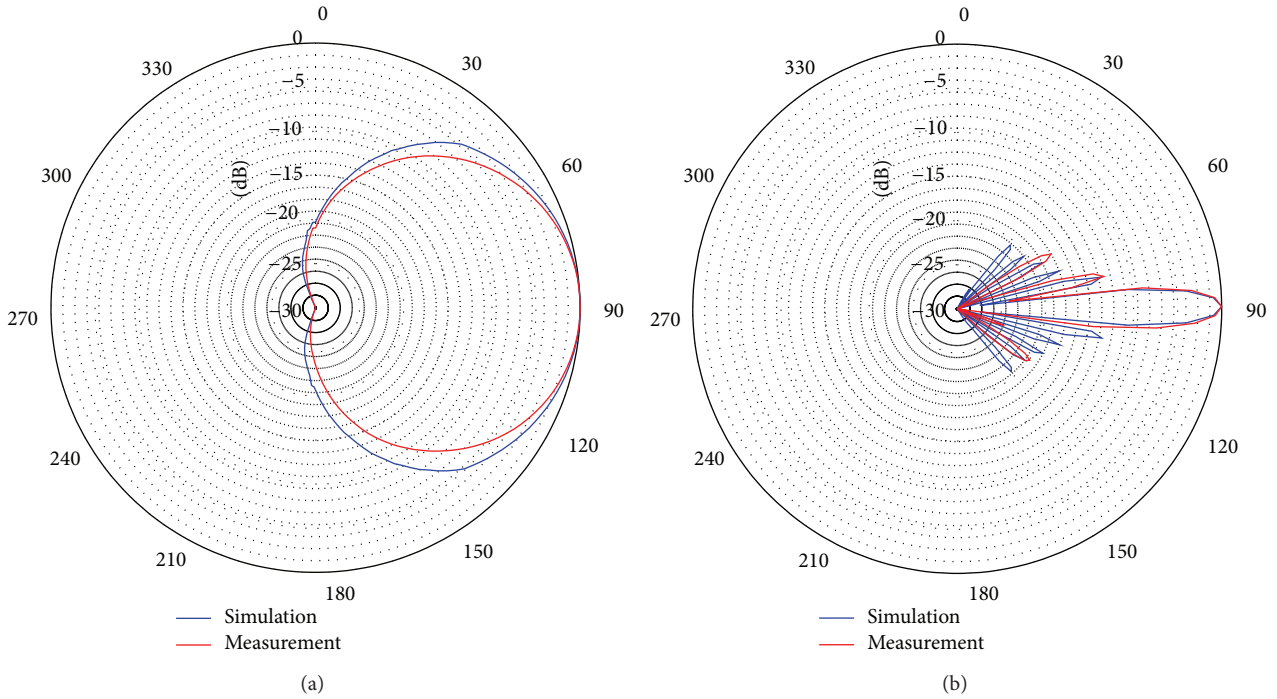

Figure 6: Comparison of radiation patterns at 1920 MHz on the horizontal and vertical planes obtained by FDTD method and measurement. (a) Horizontal plane (ϕ). (b) Vertical plane (θ).

down-tilting angle of each LTE base station antenna is 8 degrees with respect to the vertical plane. These 123 test sites were on a horizontal plane with a height of 1 meter above the ground plane. The LTE base station antenna tower located at the center of the urban area marked with a red sign having a height of 29 meters from the ground plane was constructed on the roof-floor of an eight-storey building. The relative dielectric constants, conductivities, and relative permeabilities at 1795 MHz used for modeling the ground and building are adopted to be ($\varepsilon_r = 2.55$, $\sigma = 2.64 \times 10^{-3}$ S/m,

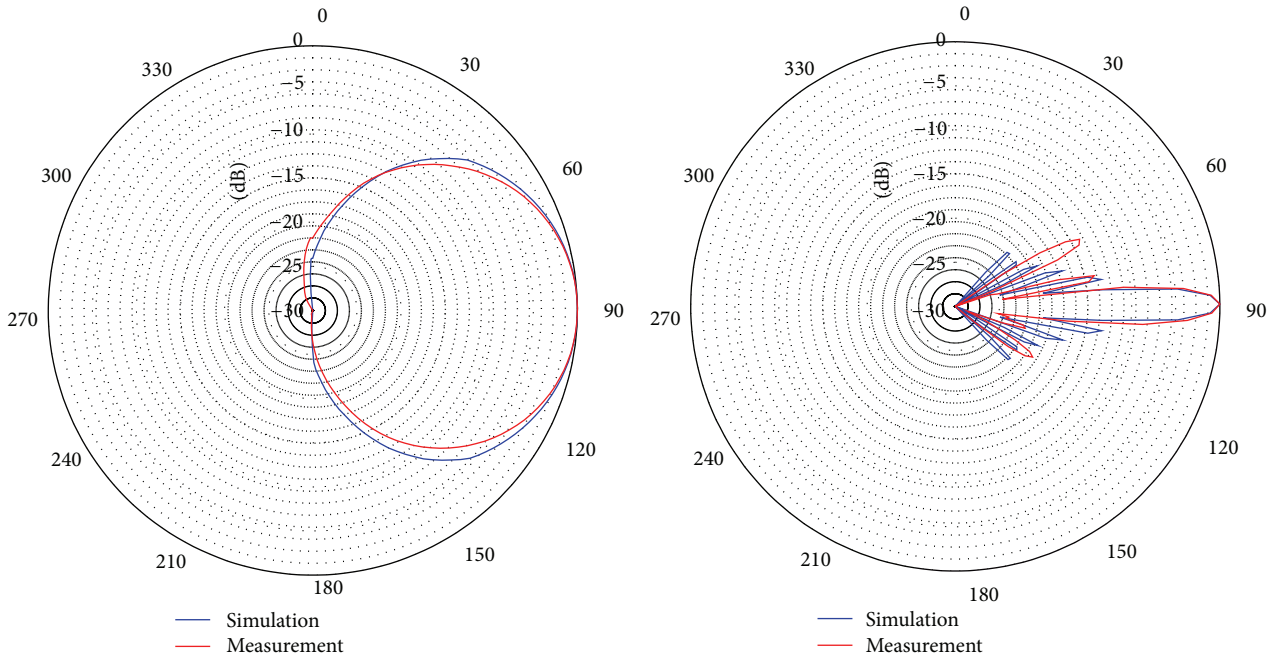

Figure 7: Comparison of radiation patterns at 2060 MHz on the horizontal and vertical planes obtained by FDTD method and measurement. (a) Horizontal plane (ϕ). (b) Vertical plane (θ).

Figure 8: An urban area of Taipei City with 123 test sites numbered from 1 to 123. The LTE base station is located at the center of the urban area marked with a red sign A.

$\mu_r = 1.0$) and ($\varepsilon_r = 3.25$, $\sigma = 1.147 \times 10^{-3}$ S/m, $\mu_r = 50$) [32–34], respectively. Measurements of the field strengths were obtained by using a Narda Model NBM-3006 high frequency selective radiation meter [35] as shown in Figure 9. The Model NBM-3006 with an isotropic E-field probe is designed to measure RF fields over the frequency range from 420 MHz to 6.0 GHz. Comparison of simulated and measured electric fields is shown in Figure 10. The simulation result of electric field distribution for the LTE base station antenna with a down-tilting angle of 8 degrees has a good agreement with the measurement data. The measured and simulated electric field strengths on a horizontal plane with a height of 1 meter above the ground are in the range of 0.098–1.179 and 0.104–1.182 V/m, respectively. Since the basic sensitivity requirement for a mobile terminal is about −100 dBm, the minimum power density of about −20 dBm obtained inside the coverage area of the LTE base station means a good signal will be picked up in the urban area. According to ANSI/IEEE standards for public exposure in uncontrolled environments, the maximum permissible exposure at 1795 MHz should be below 1.197 mW/cm^2. It is clear that the maximum power density emitted from the LTE base station is about 1.853×10^{-4} mW/cm^2 which is far below the ANSI/IEEE standard for public exposure.

7. Conclusions

In this study, we first used the FDTD method and the near zone to far zone transformation technique to simulate radiation patterns of a LTE base station antenna on vertical and horizontal planes at frequencies of 1795, 1920, and 2060 MHz, respectively. The validity of simulation results of radiation patterns was further checked by measurement data. The FDTD method and the near zone to far zone transformation technique, of which the accuracy had been validated, as well as boundary conditions were used to calculate electric fields at 123 test sites around a LTE base station in an urban area of Taipei City at 1795 MHz. Simulated electric fields

(a) (b)

Figure 9: The Narda Model SRM-3006 high frequency selective radiation meter with an isotropic E-field probe. (a) The Narda Model SRM-3006 E-field meter. (b) Isotropic E-field probe with three axis antennas.

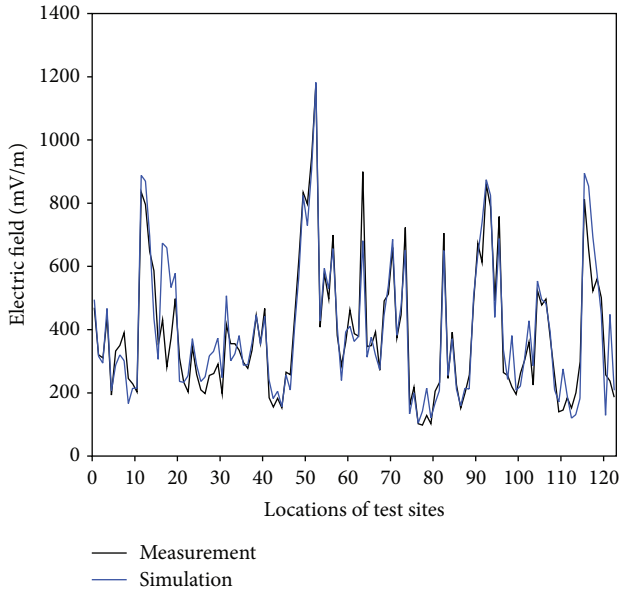

Figure 10: Comparison of simulated and measured electric field distributions. Simulated results are carried out for the LTE base station antenna with a down-tilting angle of 8 degrees and measured data is performed for the LTE base station antenna with a down-tilting angle of 8 degrees.

were compared with measured data obtained by a Narda Model SRM-3006 high frequency selective radiation meter with an isotropic E-field probe. It is found that an excellent agreement between simulated and measured data is achieved. Simulated and measured electric fields in the urban area are in the range of 0.104–1.182 and 0.098–1.179 V/m at 1795 MHz, respectively. From obtained electric field strengths, it is clear that a good signal inside the coverage area of the LTE base station in the urban area is ensured. Corresponding to the maximum electric field strength of 1.182 V/m in the urban area, the maximum power density emitted from the LTE base station is 1.853×10^{-4} mW/cm^2 and is thus far below the ANSI/IEEE standard for maximum permissible exposure of 1.197 mW/cm^2. This research work provides a time efficient and cost-effective solution to calculate electric fields emitted from LTE base stations in an urban area without measurements and to check the safety distance for public exposure to LTE base stations.

Conflict of Interests

The authors declare that there is no conflict of interests regarding the publication of this paper.

Acknowledgments

The authors would like to thank the Far EasTone Telecommunications Co. Ltd. for providing the LTE base station used for field measurements in the urban area of Taipei City. The valuable help of their manager Scott Hsu is gratefully appreciated. The authors are also grateful to Ericsson Taiwan Ltd. for providing a LTE base station antenna for measurements of radiation patterns in Yuan Ze anechoic chamber.

References

[1] "LTE-Advanced: The 3rd Generation Partnership Projected," 2011, http://www.3gpp.org/technologies/keywords-acronyms/97-lte-advanced.

[2] S. Sesia, I. Toufik, and M. Baker, *LTE—The UMTS Long Term Evolution: From Theory to Practice*, Including Release 10 for LTE-Advanced, John Wiley & Sons, New York, NY, USA, 2nd edition, 2011.

[3] F. Khan, *LTE for 4G Mobile Broadband-Air Interface Technologies and Performance*, Cambridge University Press, New York, NY, USA, 2009.

[4] "IEEE standard for safety levels with respect to human exposure to radio frequency electromagnetic fields, 3 kHz to 300 GHz," IEEE Standard C95.1, 2005.

[5] ICNIRP, "Guidelines for limiting exposure to time-varying electric, magnetic and electromagnetic fields," *Health Physics*, vol. 74, no. 4, pp. 494–522, 1998.

[6] NCRP, "Biological effects and exposure criteria for radiofrequency electromagnetic fields," NCRP Report 86, NCRP, Bethesda, Md, USA, 1986.

[7] R. C. Petersen and P. A. Testagrossa, "Radio-frequency electromagnetic fields associated with cellular-radio cell-site antennas," *Bioelectromagnetics*, vol. 13, no. 6, pp. 527–542, 1992.

[8] E. D. Mantiply, K. R. Pohl, S. W. Poppell, and J. A. Murphy, "Summary of measured radiofrequency electric and magnetic fields (10 kHz to 30 GHz) in the general and work environment," *Bioelectromagnetics*, vol. 18, no. 8, pp. 563–577, 1997.

[9] A. Thansandote, G. B. Gajda, and D. W. Lecuyer, "Radiofrequency radiation in five Vancouver schools: exposure standards not exceeded," *CMAJ*, vol. 160, no. 9, pp. 1311–1312, 1999.

[10] H.-Y. Chen, T.-Y. Su, and C.-Y. Chuang, "Electric fields radiated from a cellular phone base station antenna constructed on a roof-top," *Electromagnetics*, vol. 29, no. 3, pp. 235–249, 2009.

[11] K. S. Yee, "Numerical solution of initial boundary value problems involving Maxwells equations in isotropic media," *IEEE Transactions on Antennas and Propagation*, vol. 14, no. 5, pp. 302–307, 1966.

[12] R. J. Luebbers, K. S. Kunz, M. Schneider, and F. Hunsberger, "A finite-difference time-domain near zone to far zone transformation," *IEEE Transactions on Antennas and Propagation*, vol. 39, no. 4, pp. 429–433, 1991.

[13] A. Taflove and M. E. Brodwin, "Numerical solution of steady-state electromagnetic scattering problems using the time-dependent Maxwell's equations," *IEEE Transactions on Microwave Theory and Techniques*, vol. 23, no. 8, pp. 623–630, 1975.

[14] G. Mur, "Absorbing boundary conditions for the finite-difference approximation of the time-domain electromagnetic field equation," *IEEE Transactions on Electromagnetic Compatibility*, vol. 23, no. 4, pp. 377–382, 1981.

[15] Z. Liao, H. L. Wong, Y. Baipo, and Y. Yuan, "A transmitting boundary for transient wave analysis," *Scientia Sinica*, vol. 27, no. 10, pp. 1063–1076, 1984.

[16] J.-P. Berenger, "A perfectly matched layer for the absorption of electromagnetic waves," *Journal of Computational Physics*, vol. 114, no. 2, pp. 185–200, 1994.

[17] S. A. Schelkunoff, "Some equivalence theorems of electromagnetics and their application to radiation problems," *Bell System Technical Journal*, vol. 15, pp. 92–112, 1936.

[18] C. Huygens, *Traite de la Lumiere*, Vander Aa, Leiden, The Netherlands, 1690, (Translated into English by S. P. Thompson, London, UK, 1912, reprinted by the University of Chicago Press).

[19] J. D. Kraus and K. R. Carver, *Electromagnetics*, McGraw-Hill, New York, NY, USA, 2nd edition, 1973.

[20] C. A. Balanis, *Antenna Theory-Analysis and Design*, John Wiley & Sons, New York, NY, USA, 3rd edition, 2005.

[21] D. E. Livesay and K. M. Chen, "Electromagnetic field induced inside arbitrarily shaped biological bodies," *IEEE Transactions on Microwave Theory and Techniques*, vol. 22, no. 12, pp. 1273–1280, 1974.

[22] K. Karimullah, *Theoretical and experimental study of the proximity effects of thin-wire antenna in presence of biological bodies [Dissertation]*, Michigan State University, East Lansing, Mich, USA, 1979.

[23] *Kathrein Panel Antenna, Type 742214V01*, Kathrein Inc., Rosenheim, Germany, 2013, http://www.kathrein-scala.com/catalog/742214V01.pdf.

[24] ETSI, "Universal mobile telecommunications system (UMTS); spacial channel model for multiple input multiple output (MIMO) simulations," Tech. Rep. 25.996 Version 6.1.0 Release 6, European Telecommunications Standards Institute, Sophia Antipolis, Cedex, France, 2003.

[25] D. J. Y. Lee and C. Xu, "Mechanical antenna downtilt and its impact on system design," in *Proceedings of the 47th IEEE Vehicular Technology Conference*, pp. 447–451, Phoenix, Ariz, USA, May 1997.

[26] I. Forkel, A. Kemper, R. Pabst, and R. Hermans, "The effect of electrical and mechanical antenna down-tilting in UMTS networks," in *Proceedings of the 3rd International Conference on 3G Mobile Communication Technologies*, pp. 86–90, Gdansk, Poland, May 2002.

[27] J. Niemelä and J. Lempiäinen, "Impact of mechanical antenna downtilt on performance of WCDMA cellular network," in *Proceedings of the IEEE 59th Vehicular Technology Conference*, vol. 4, pp. 2091–2095, Milan, Italy, May 2004.

[28] J. Niemelä and J. Lempiäinen, "Mitigation of pilot pollution through base station antenna configuration in WCDMA," in *Proceedings of the IEEE 60th Vehicular Technology Conference*, vol. 6, pp. 4270–4274, IEEE, Milan, Italy, September 2004.

[29] L. Manholm, M. Johansson, and S. Petersson, "Influence of electrical beamtilt and antenna beamwidths on downlink capacity in WCDMA: simulations and realization," in *Proceedings of the IEEE International Symposium on Antennas and Propagation*, pp. 641–644, Sendai, Japan, 2004.

[30] S. C. Bundy, "Antenna downtilt effects on CDMA cell-site capacity," in *Proceedings of the IEEE Radio and Wireless Conference (RAWCON 99)*, pp. 99–102, Denver, Colo, USA, 1999.

[31] K. C. Gupta and P. S. Hall, *Analysis and Design of Integrated Circuit-Antenna Modules*, John Wiley & Sons, New York, NY, USA, 2000.

[32] A. von Hippel, *Dielectric Materials and Applications*, The MIT Press, Cambridge, Mass, USA, 1954.

[33] J. Horikoshi, K. Tanaka, and T. Morinaga, "1.2 GHz band wave propagation measurements in concrete building for indoor radio communications," *IEEE Transactions on Vehicular Technology*, vol. 35, no. 4, pp. 146–152, 1986.

[34] E. C. Jordan, *Reference Data for Engineers: Radio, Electronics, Computer, and Communications*, Howard W. Sams & Company, Indianapolis, Ind, USA, 7th edition, 1985.

[35] Narda Safety Test Solutions, Hauppauge, NY, USA.